13th International Symposium on Turbulence and Shear Flow Phenomena (TSFP13)
Montreal, Canada, June 25–28, 2024

EFFECT OF FLOW HISTORY IN TURBULENT BOUNDARY LAYERS WITH ADVERSE PRESSURE GRADIENT

Taygun Recep Gungor
Department of Mechanical Engineering
Laval University
Quebec City, QC, G1V 0A6 Canada
taygun-recep.gungor.1@ulaval.ca

Ayse Gul Gungor
Faculty of Aeronautics and Astronautics
Istanbul Technical University
34469, Istanbul, Turkey
ayse.gungor@itu.edu.tr

Yvan Maciel
Department of Mechanical Engineering
Laval University
Quebec City, QC, G1V 0A6 Canada
yvan.maciel@gmc.ulaval.ca

ABSTRACT

The mean velocity and Reynolds stress profiles from three non-equilibrium pressure-gradient turbulent boundary layers that are generated using direct numerical simulation are examined to further understand the effect of flow history. The pressure force impact on the inner and outer regions is represented by two parameters: the friction-viscous pressure-gradient parameter, β_i, and the pressure-gradient parameter based on Zagarola-Smits velocity, β_{ZS}, respectively. In all three flow cases, both β_i and β_{ZS} exhibit similar distributions, initially increasing and then decreasing. However, the rate of change of these parameters along the streamwise direction varies among the flows, indicating differing levels of pressure force disequilibration. In addition, we employ two near-equilibrium cases with minimal variations of the pressure gradient parameters for comparisons. The study aims to isolate the three effects of the pressure force on the inner and outer layers: local direct impact (β value), local disequilibrating effect ($d\beta/dx$ value), and upstream cumulative effect, while accounting for the inevitable Reynolds number effect. In the outer layer, it is found that both the local and cumulative disequilibrating effects modify the mean velocity and Reynolds stress profiles at identical β_{ZS} values. The faster the variations in pressure force impact, the more delayed the response of both mean flow and turbulence. Cumulative effects prove to be significant. In the inner layer, which responds much faster to changes in pressure force, the local disequilibrating effect still modifies the mean velocity profile in the viscous sublayer. Notably, in situations where the mean velocity defect is significant, the behavior of turbulence in the inner layer appears to be dictated by how outer turbulence responds to pressure force effects.

INTRODUCTION

The development of a turbulent boundary layer (TBL) under the influence of an adverse pressure gradient (APG) exhibits distinct characteristics from those observed in canonical wall-bounded flows, such as channel and pipes flows, or TBLs with zero pressure gradient. This difference becomes particularly pronounced under conditions of a strong pressure gradient or prolonged exposure to it, significantly altering the mean flow behavior and, subsequently, the turbulence characteristics. The technological relevance of APG TBLs has spurred numerous studies aimed at elucidating the impact of APG on flow dynamics and turbulence. Despite extensive research efforts, several aspects of APG TBLs are only poorly understood and many questions still remain unanswered.

A critical, yet unresolved, aspect concerns the influence of flow history on the mean flow and turbulence characteristics within APG TBLs. This challenge stems from the inherent complexities in decoupling the historical effects of flow from other influencing parameters, such as the Reynolds number or the local force balance. While existing literature attempts to shed light on this matter, such as the study of Bobke *et al.* (2017), there is an evident gap in adopting a systematic approach to rigorously explore this issue. The databases in the literature often have arbitrary PG distributions with varying features. Moreover, documented flow cases typically exhibit minimal velocity defects, rendering the isolation of pressure gradient effects from those attributable to Reynolds number variations as particularly challenging.

This study seeks to delineate the influence of flow history, as well as the local disequilibrium effect of the pressure force, on mean flow and turbulence in non-equilibrium APG TBLs reaching large velocity defects. To achieve this objective, we utilize several databases from the literature. The first two databases (D16 and D22) are highly non-equilibrium APG TBLs of Gungor *et al.* (2016) and Gungor *et al.* (2022). The Reynolds number based on the momentum thickness (Re_θ) of these cases reaches 4650 and 8650, respectively. The third one (D23) is the flow case of Gungor *et al.* (2024). Differently from the previous two TBLs, D23 is exposed to an APG first, followed by a favorable pressure gradient (FPG). The Reynolds number for this flow is the highest, with Re_θ ranging from 1940 to 13000. The first two flows, as well as the initial APG region of the third, exhibit an initial increase followed by a decrease in pressure force impact, resulting in continuous momentum loss. However, in the FPG region of D23, the flow begins to regain momentum. Nevertheless, our study primarily focuses on the APG region of D23. In addition to these non-

equilibrium TBLs, we also include the two near-equilibrium cases from Kitsios *et al.* (2017) with mild and strong APGs (EQ1 and EQ2, respectively). This inclusion allows for a better distinction between the direct local impact of the pressure force and its cumulative effect.

The selected databases span a broad spectrum of velocity defect conditions, from a very-small defect TBL, almost like a zero PG TBL, to a large defect TBL. This allows us to examine the effect of flow history in different flow conditions. We utilize the mean flow and Reynolds stresses along with the local force balance and the change of the force balance to understand the flow history.

METHODOLOGY

The flow dynamics are influenced by three distinct pressure gradient effects (Gungor *et al.*, 2024): the local pressure force, its variation (local disequilibrating effect), and upstream history. For examining the force balance, we utilize the mean momentum equation budgets. The streamwise mean momentum equation where each term can be considered as a force acting on the flow is

$$0 = \left(-U\frac{\partial U}{\partial x} - V\frac{\partial U}{\partial y} \right) - \frac{1}{\rho}\frac{dp_e}{dx} - \frac{\partial \langle uv \rangle}{\partial y} + \nu\frac{\partial^2 U}{\partial y^2} \quad (1)$$

where U and V are the mean velocities in the streamwise and wall-normal directions, ρ is the density, p_e is the pressure at the edge of the boundary layer, u and v are the fluctuation velocities, ν is the viscosity and $\langle . \rangle$ indicates ensemble averaging. The terms on the right-hand side of the equation represent the inertia force, the pressure force, the apparent turbulent force (the gradients of the normal stresses are not considered because they are negligible) and the viscous force, respectively.

The force balance in the inner and outer layers can be significantly different from each other and due to this, we examine the force balance in each layer separately. For the outer layer, we employ the PG parameter based on the Zagarola–Smits velocity (U_{ZS}), $\beta_{ZS} = (\delta/\rho U_{ZS}^2)(dp_e/dx)$, where δ is the local boundary layer thickness. It accurately depicts the ratio of the pressure force to the turbulent force in the outer layer in APG TBLs (Maciel *et al.*, 2018; Gungor *et al.*, 2024). As for the inner layer, we utilize the inner-layer PG parameter, $\beta_i = (\nu/(\rho u_\tau^3))(dp_w/dx)$, which represents the ratio of pressure force to turbulent force within the inner layer. Here, p_w stands for wall pressure and u_τ for friction velocity.

The second PG effect that influences the flow is the local disequilibrating effect. This can be explained as the change rate of the force balance. We investigate this effect using the derivative of the corresponding PG parameters in the streamwise direction: $d\beta/dX$, where $X = x/L$ and L is the reference streamwise length. Unfortunately, as discussed by Maciel *et al.* (2018), L cannot be easily defined if one wants to compare non-equilibrium TBLs evolving on flat plates. We choose L as the average boundary layer thickness in the region of interest (δ_{av}) in the outer layer, as in Maciel *et al.* (2018) and friction-viscous scales in the inner layer.

Figure 1 shows the spatial evolution of the main flow parameters as a function of x/δ_{av} for the three non-equilibrium TBLs. The three flow cases have a similar spatial evolution of β_{ZS}. The parameter β_{ZS}, which reflects the local direct impact of the pressure force on the outer layer, initially rises and subsequently falls. An increase of β_{ZS} represents a momentum-losing effect of the PG in the outer region, although such an

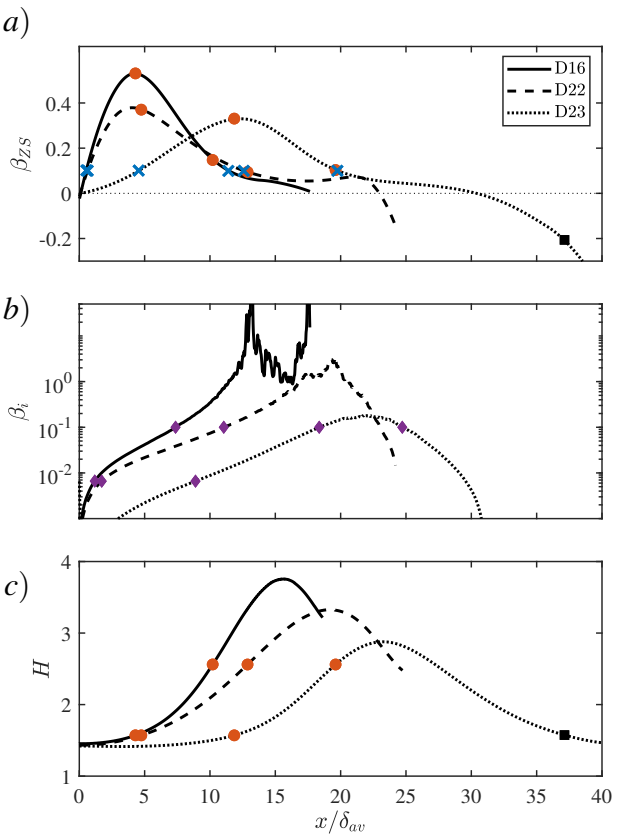

Figure 1. The β_{ZS}, H, and β_i distribution of the non-equilibrium flow cases.

effect is not instantaneous due to the delayed response of the mean flow (Gungor *et al.*, 2024). Conversely, a decrease of β_{ZS} signifies a momentum-gaining effect. β_{ZS} increases faster in D16, denoting a stronger disequilibrating effect of the PG. This variation in the distribution of β_{ZS} across the cases leads to different shape factor distributions, as illustrated in Figure 1(c). As anticipated, the rise in the shape factor H correlates with the intensity of the change in β_{ZS} in the streamwise direction, $d\beta_{ZS}/dX$. The delayed response of the mean flow can also be observed in this figure.

Figure 1(b) presents β_i distribution as a function of x/δ_{av}. The β_i values vary considerably across all cases, necessitating the scaling of the y-axis on a logarithmic scale. The effect of the pressure force on the inner layer is clearly different from the one in the outer layer. Whereas the relative importance of the pressure force with respect to the turbulent force begins to decline in the outer layer even before the middle of the domain, it keeps increasing in the inner layer much longer. This highlights the necessity of conducting separate analyses for the inner and outer layers.

RESULTS

Outer layer

We start investigating the outer layer by comparing the three non-equilibrium flows at two streamwise positions with the same β_{ZS} value, $\beta_{ZS} = 0.1$, in the increasing-β_{ZS} and decreasing-β_{ZS} zones. These six streamwise positions are marked in figure 1a with blue cross marks. This value of β_{ZS} was selected to enable comparison between cases at the beginning of the domain, where flow history is still small. The main parameters of these cases are listed in Table 1. In the cases

Table 1. The main properties of cases with same β_{ZS}

Name	β_{ZS}	$d\beta_{ZS}/d(x/\delta_{av})$	Re_{ZS}
D16 - $\beta_{ZS}\uparrow$	0.10	0.197	220
D22 - $\beta_{ZS}\uparrow$	0.10	0.153	361
D23 - $\beta_{ZS}\uparrow$	0.10	0.035	588
D16 - $\beta_{ZS}\downarrow$	0.10	-0.032	4692
D22 - $\beta_{ZS}\downarrow$	0.10	-0.020	5712
D23 - $\beta_{ZS}\downarrow$	0.10	-0.023	10290

where β_{ZS} increases (momentum-losing effect), the increase is more pronounced for D16 and much milder for D23. Conversely, in the three cases where β_{ZS} decreases (momentum-gaining effect), the decrease is small and similar for all three flows.

Figure 2a presents the outer-scaled mean velocity profiles (U/U_e, where U_e is the local edge velocity) of the six cases as a function of y/δ. The first three flow cases (blue lines in the figure) provide an opportunity to see the effect of $d\beta_{ZS}/dX$ with minimal history effects, since they are near the beginning of their respective flow domain. The difference between the three mean velocity profiles follows the expected trend: the defect increases from D16 to D23 because the mean flow cannot respond instantaneously to the increase in the pressure force. Specifically, the rapid increase in β_{ZS} for D16 means that the mean flow has had less time to react compared to the other two flows. It's worth noting that the Reynolds number effect (lower $Re_{ZS} = (\delta U_{ZS}/\nu)(U_{ZS}/U_e)$ for D16 and D22 compared to D23) tends to reduce these differences, as the mean velocity profiles become fuller at higher Reynolds numbers. As shown in figure 2b, the $\langle u^2 \rangle$ profiles are similar and the trend is not conclusive as the Reynolds number plays an important role for the Reynolds stresses.

In the three downstream cases (orange lines in figure 2), β_{ZS} remains identical, and $d\beta_{ZS}/dX$ is similar. This allows for the almost complete isolation of the flow history effect, which is significant in these cases, but Reynolds number effects are also present. Figure 2a illustrates that the cumulative effect of the APG results in a significant velocity defect in these three cases. D16 exhibits the largest velocity defect, partly due to higher upstream β_{ZS} values and partly because of the lower Reynolds number. The differences between D22 and D23 are small as they have more similar upstream histories and Reynolds numbers. Nonetheless, the larger velocity defect for D23 suggests a stronger upstream impact of the PG.

As for the $\langle u^2 \rangle$ profiles for these three cases, they are typical of strong APG cases with important outer layer turbulence and the absence of an inner peak. The higher levels of $\langle u^2 \rangle$ for D16 are expected due to the strong upstream impact of the APG, while the lower Reynolds number may also contribute. The observation that $\langle u^2 \rangle$ levels are higher for D23 than D22 is consistent with the slightly larger mean velocity defect of D23, again suggesting a stronger upstream impact of the APG.

For a different perspective, we also compare the APG TBLs at the same shape factor as it takes the cumulative effect of the pressure gradient into account. We choose two values of the shape factor, $H = 1.57$ and 2.56, which correspond to the values of the near-equilibrium TBLs of Kitsios *et al.* (2017), to incorporate these cases into our analysis. By doing so, we can compare the non-equilibrium TBLs with APG TBL cases

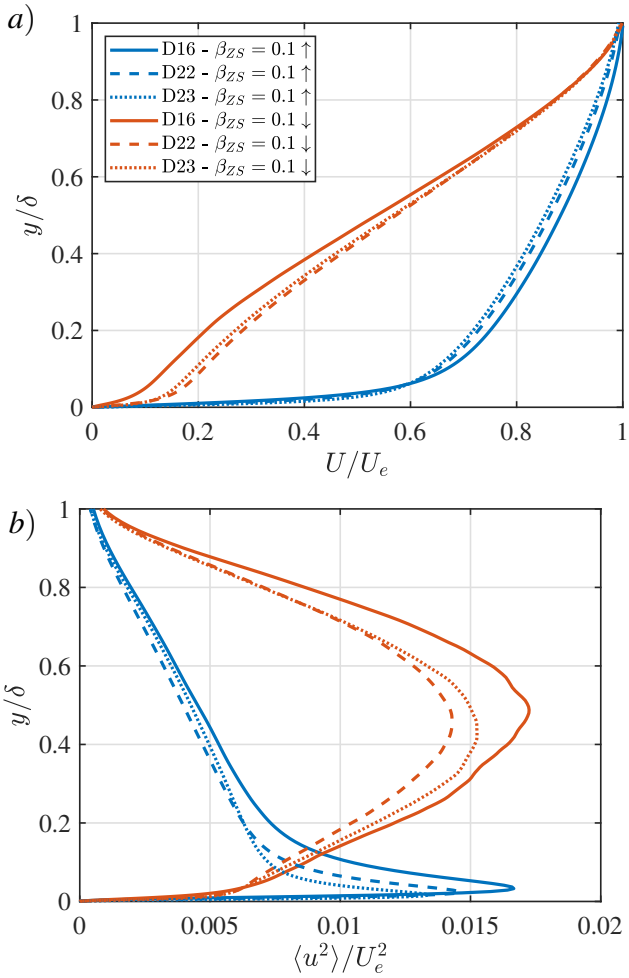

Figure 2. The outer-scaled scaled mean velocity (a) and $\langle u^2 \rangle$ (b) profiles of several streamwise positions with the same β_{ZS} values as a function of y/δ. The arrow indicates the change rate of β_{ZS}.

where the influence of flow history is minimal. The mean velocity defect is small for $H = 1.57$ and large for $H = 2.56$. We also have another position further downstream in D23 (FPG) where H also equals 1.57, but with a favorable pressure gradient (both β_{ZS} and $d\beta_{ZS}/dX$ are negative). The selected positions for the non-equilibrium cases are marked with orange circles for the APG cases and a black square for the FPG case in figure 1. The main properties of these cases are given in Table 2.

We begin by analyzing the force balance for the non-equilibrium TBLs. The near-equilibrium TBLs cannot be included due to the unavailability of their momentum budget data. Figure 3 presents the outer-scaled mean momentum budgets. The momentum budget terms are normalized with the pressure force to facilitate comparison between the two defect situations. Despite different upstream histories among the three databases, the wall-normal distribution of the force balance at a given H value is strikingly similar, showing near-collapse. This suggests that the force balance can be directly correlated with H when both β_{ZS} and $d\beta_{ZS}/dX$ are similar, and when the upstream flow history is similar in trend, as it is the case for the two triads of APG cases considered here. However, the mean momentum budget for the FPG case, illustrated in figure 3a, clearly shows that this is no longer true when the

Table 2. The main properties of cases with same H.

Name	H	β_{ZS}	$d\beta_{ZS}/d(dx/\delta_{av})$	Re_{ZS}
D16	1.57	0.53	-0.005	488
D22	1.57	0.37	-0.020	839
D23	1.57	0.33	0.006	1622
EQ1	1.57	0.12	≈ 0	1151
FPG	1.57	0.20	-0.049	4616
D16	2.56	0.14	-0.049	3433
D22	2.56	0.09	-0.019	6029
D23	2.56	0.10	-0.024	10051
EQ2	2.56	0.08	≈ 0	8488

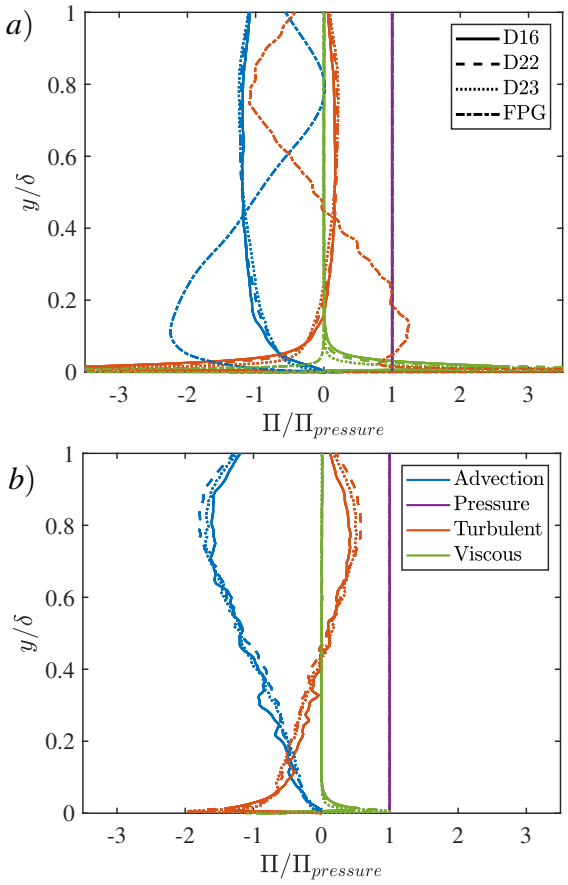

Figure 3. The terms of the mean momentum budget profiles of the small defect (a) and large defect cases (b) as a function of y/δ for D16 (straight), D22 (dashed) and D23 (dotted) and the FPG case (dashed-dotted).

local pressure force and upstream history are completely different.

The mean velocity profiles are depicted in figure 4a, alongside the two near-equilibrium TBLs (EQ1 and EQ2), and the ZPG TBL ($Re_\tau = 1306$) from Sillero *et al.* (2013) for reference.

Beginning with the four APG TBLs exhibiting a small defect ($H = 1.57$; indicated by the green lines), we observe that while the profiles are grouped together, they are not identical, despite being APG cases with the same shape factor. The trend indicates an increasing momentum defect in the outer layer as we progress from the stronger disequilibrium case D16 to the near-equilibrium case EQ1. This trend is primarily attributed to the disequilibrium APG history of the flows, although it may also be partly influenced by the varying local impact of the pressure gradient, as indicated by the β_{ZS} values in Table 2. These values decrease from D16 to D22, to D23, to EQ1. Additionally, the lower Reynolds number of D16 accentuates these differences. Since $d\beta_{ZS}/dX$ is small and similar for all non-equilibrium cases, the local destabilizing effect of the pressure gradient is likely minimal here.

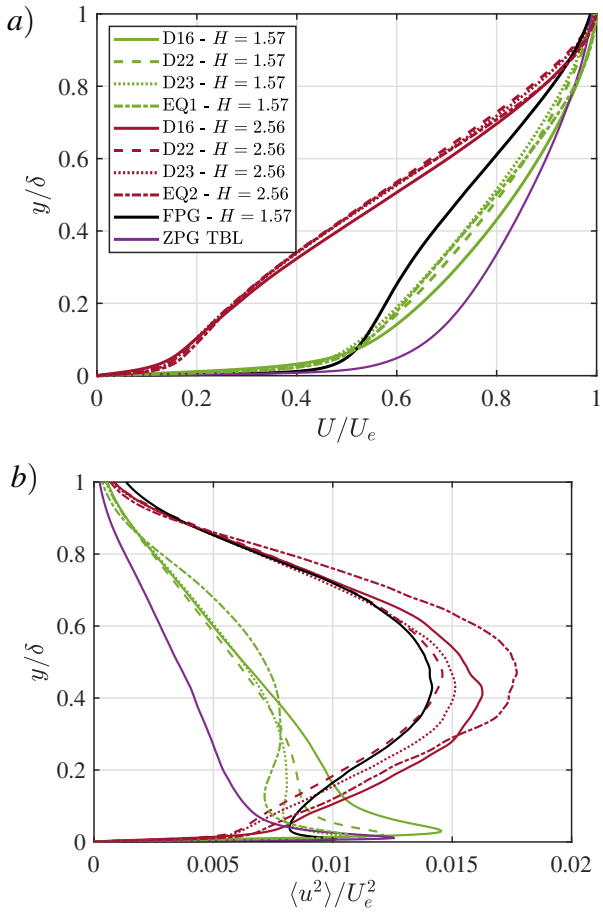

Figure 4. The outer-scaled scaled mean velocity (a) and $\langle u^2 \rangle$ (b) profiles of several streamwise positions with the same shape factor along with the ZPG TBL case of Sillero *et al.* (2013) as a function of y/δ.

A clear and significant effect of flow history is evident in the FPG profile at the same H value (indicated by the black line). It is important to note that an equilibrium FPG TBL can never exhibit such a significant defect (a high H value) as the non-equilibrium FPG case depicted in the figure. Equilibrium FPG TBLs always have fuller profiles than the ZPG TBL (purple line), regardless of β_{ZS} value. The current FPG TBL is recovering from the pronounced upstream cumulative APG effects. As it regains momentum, it does so faster near the wall than in the outer region, resulting in a velocity profile shape markedly different from those of the four small-defect APG cases.

The scenario for the four large-defect APG TBLs (indicated by the red lines) mirrors that of the small-defect cases, albeit with smaller differences and a less clear trend. In this case, the β_{ZS} values are similar for all four TBLs.

Figure 4b presents the $\langle u^2 \rangle$ profiles as a function of y/δ for the same APG cases discussed above. In the small-defect cases, the inner-layer turbulence is still dominant. The inner peak's levels are higher than outer-layer levels. However, the outer-layer turbulence is elevated in all cases with respect to that in the ZPG TBL. Despite this similarity, the differences in the $\langle u^2 \rangle$ profiles are more pronounced than those of the mean velocity profiles. Firstly, the broader inner peak for D16 reveals a significant Reynolds number effect in the lower part of this boundary layer. However, overall, the non-equilibrium TBLs do not exhibit the outer-layer plateau of the near-equilibrium TBL, between $y/\delta = 0.3$ and 0.4, even if their β_{ZS} values are higher than that of EQ1. This indicates a delay in turbulence response to the cumulative effect of the pressure gradient, consistent with the findings of Gungor *et al.* (2024).

The $\langle u^2 \rangle$ profile of the FPG TBL shows an even greater history effect. It resembles those of the large-defect TBLs, indicating that turbulence has not yet recovered from the upstream APG effects. In an equilibrium FPG TBL, the $\langle u^2 \rangle$ level in the outer region would be lower than that of the ZPG TBL.

In the large-defect case, the inner peak of the $\langle u^2 \rangle$ profiles vanishes and the outer-layer turbulent activity becomes dominant. Differently from what we observe for the small-defect cases, the wall-normal distribution of the $\langle u^2 \rangle$ profiles is very similar to each other. The $\langle u^2 \rangle$ levels of the non-equilibrium TBLs are nonetheless lower than that of the near-equilibrium case, indicating again a delayed response of turbulence.

Inner layer

For the inner layer comparison, we examine flows at identical values of the inner-layer PG parameter, β_i. Thus, we select positions in the non-equilibrium TBLs with the same β_i values as the near-equilibrium TBLs: $\beta_i = 0.0066$ and 0.1000. The streamwise positions of the non-equilibrium cases are indicated in Figure 1b with diamond symbols. They are located in a region where β_i increases, except for the third position in D23. The main parameters of these cases are listed in Table 3.

Table 3. The main properties of cases with same β_i

Name	β_i	$d\beta_i/dx^+ \times 10^4$	Re_τ	
D16 - Low β_i	0.0066	0.0521	427	—
D22 - Low β_i	0.0066	0.0208	581	- -
D23 - Low β_i	0.0066	0.0068	957	····
EQ1 - Low β_i	0.0066	≈ 0	793	—·
D16 - High β_i	0.1000	0.9046	411	—
D22 - High β_i	0.1000	0.4396	538	- -
D23 - High β_i	0.1000	0.3365	800	····
D23 - High β_i	0.1000	-0.6552	831	····
EQ2 - High β_i	0.1000	≈ 0	691	—·
ZPG	0	0	1306	—

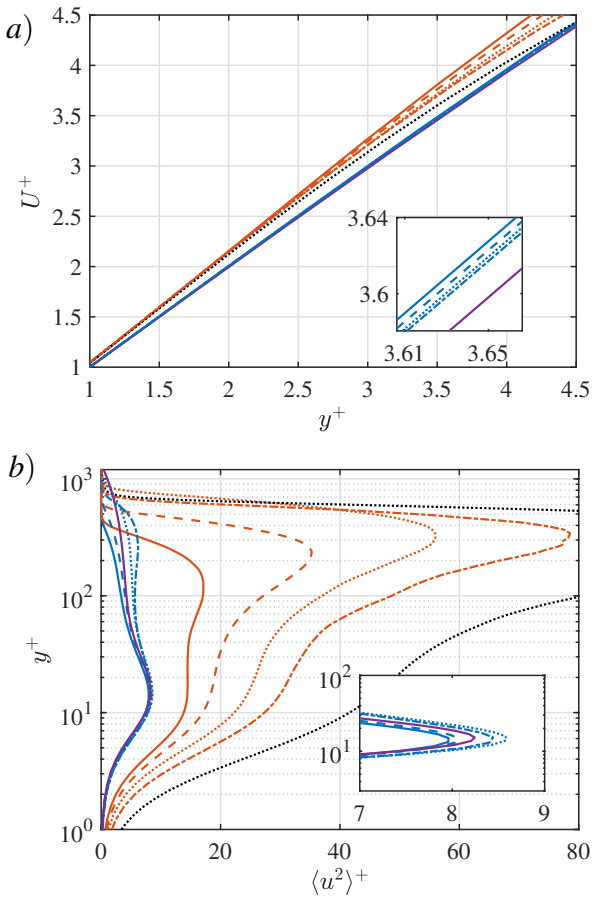

Figure 5. The friction-viscous scaled mean velocity (a) and $\langle u^2 \rangle$ (b) profiles of several streamwise positions with the same β_i value as a function of y^+. The legend is given in Table 3.

Figure 5a shows U^+ as a function of y^+ in the viscous sublayer for all these cases along with the ZPG TBL. Since inertia effects are minimal in the near-wall region, as expected, the profiles tend to cluster together for a given value of β_i. At the low β_i value (0.0066), they nearly collapse, slightly above the ZPG TBL profile. However, the inset in Figure 5a, zooming in on the region around $y^+ = 3.64$, reveals a slight trend. Given the rapid response of the near-wall region to changes, this is likely more indicative of a local disequilibrating effect ($d\beta_i/dx^+$) than a cumulative effect. The fact that U^+ increases with increasing $d\beta_i/dx^+$ tends to support this hypothesis.

A similar trend is observed for the high β_i cases ($\beta_i = 0.1$), but it is much more pronounced. Once again, U^+ increases with increasing $d\beta_i/dx^+$. Additionally, the black dotted curve corresponds to negative $d\beta_i/dx^+$ and lies below the near-equilibrium curve. These observations further suggest that the variations are primarily attributable to the local disequilibrating effect of the pressure gradient, although a minor historical effect may also be present

Figure 5b shows the $\langle u^2 \rangle^+$ profiles as a function of y^+. The inner peak for the $\langle u^2 \rangle$ profiles in the low-β_i cases exists in all four cases and the shape of the profiles in the inner layer are almost identical even though the outer layers behave differently from each other. The $\langle u^2 \rangle$ profile's peak is located at $y^+ \approx 14$ but there is a minor difference between the levels. Regarding this difference, we first focus on the near-equilibrium TBLs (ZPG and EQ1) to see the effect of β_i. The peak of $\langle u^2 \rangle^+$ is higher in EQ1 than in the ZPG TBL, despite EQ1 having a

considerably lower Re_τ compared to the ZPG TBL. Given that the peak level is known to increase with Reynolds number in the case of the ZPG TBL, these results suggest that positive values of β_i also contribute to an increase in the inner peak of $\langle u^2 \rangle^+$. Now, when we compare the inner peaks of the four APG TBLs at the same low β_i value, the variations do not align consistently with the changes of $d\beta_i/dx^+$. Instead, they correspond with variations in Re_τ. However, the effect of $d\beta_i/dx^+$ cannot be discarded because we cannot isolate any of these factors with the existing cases. Nonetheless, the difference in levels is small. Overall, the similarity of the $\langle u^2 \rangle$ profiles in the inner layer suggests that flow history plays a minor role in these cases.

The picture changes significantly in the high-β_i cases. The Reynolds stress levels are very different between these cases, with the same trend throughout the whole boundary layer. This phenomenon can likely be attributed to the dominance of turbulence in the outer layer in large-defect TBLs (Gungor *et al.*, 2016, 2022). Consequently, the observed increase in $\langle u^2 \rangle$ from the stronger disequilibrium case D16 to the near-equilibrium case EQ2 probably reflects historical effects in the outer region, including the delayed turbulence response. However, since these cases were selected at constant β_i, an inner-layer parameter, no definitive conclusions can be drawn from their comparison.

CONCLUDING REMARKS

In this study, we explored the effect of the flow history on the inner and outer layers of turbulent boundary layers, along with the influence of the local pressure force and its variation (local disequilibrating effect). The main conclusions are as follows:

1. First, it is important to state that the five flow cases used in this study (three non-equilibrium, two near-equilibrium) do not allow for a clear-cut separation between the four effects present, namely the three pressure force effects and the Reynolds number effect. Achieving this separation would require designing and generating numerous flow cases, each with only one of these four effects changing. However, such an extensive set of flow cases does not currently exist and would be challenging to implement. Nevertheless, because they represent three distinct degrees of flow disequilibration, the three non-equilibrium TBLs analyzed in this study offer valuable insights into these three pressure force effects.
2. By examining positions from the different flows with the same positive (APG) value of the pressure gradient parameter β_{ZS}, and located near the beginning of the flow domains, it becomes evident that the streamwise rate of change of the pressure gradient impact ($d\beta_{ZS}/dX$) influences the mean velocity profiles in the outer layer. Essentially, the mean flow does not respond instantaneously to the pressure force increase: the more rapid the increase, the more delayed is the response.
3. In another comparison where β_{ZS} was identical and $d\beta_{ZS}/dX$ was similar between flow cases, the cumulative impact of the pressure force (history effect) became apparent. A stronger cumulative APG impact resulted in a larger momentum defect and increased Reynolds stresses in the outer layer.
4. Even when comparing different APG TBLs with the same value of the shape factor, which necessarily implies mean velocity profiles that should be similar, these profiles differ slightly between flow cases. The results suggest that this is mainly due to the different APG cumulative effects rather than local effects. The differences are even more pronounced for the streamwise Reynolds normal stress, revealing a clear delay in turbulence response. The FPG TBL at the end of one flow, with the same shape factor as the small-defect APG cases considered, exemplified a drastic case of flow history effects. Its mean velocity and Reynolds stress profiles deviate considerably from those of the small-defect APG TBLs.
5. Regarding the inner layer, a comparison of the flows at identical values of the inner pressure gradient parameter β_i reveals that the friction-viscous scaled mean velocity profiles in the viscous sublayer are grouped according to the β_i value. However, even in this near-wall region where inertia effects are minimal, the profiles at identical β_i values differ slightly due to the local disequilibrating effect of the pressure gradient ($d\beta_i/dx^+$). As for the $\langle u^2 \rangle$ profile in the inner layer, the effect of the pressure gradient is minor for small values of β_i but becomes important for higher values of β_i, corresponding to a significant mean velocity defect. In the latter case, the results suggest that it is the response of outer-layer turbulence to the pressure force effects that controls what happens in the inner layer.

ACKNOWLEDGMENTS

We acknowledge PRACE for awarding us access to Marconi100 at CINECA, Italy and Calcul Québec (www.calculquebec.ca) and the Digital Research Alliance of Canada (alliancecan.ca) for awarding us access to Niagara HPC server. TRG and YM acknowledge the support of the Natural Sciences and Engineering Research Council of Canada (NSERC), project number RGPIN-2019-04194. TRG and AGG were supported by the research fund of Istanbul Technical University (project number: MDK-2018-41689)

REFERENCES

Bobke, A., Vinuesa, R., Örlü, R. & Schlatter, P. 2017 History effects and near equilibrium in adverse-pressure-gradient turbulent boundary layers. *Journal of Fluid Mechanics* **820**, 667–692.

Gungor, A.G., Maciel, Y., Simens, M.P. & Soria, J. 2016 Scaling and statistics of large-defect adverse pressure gradient turbulent boundary layers. *International Journal of Heat and Fluid Flow* **59**, 109–124.

Gungor, T.R., Gungor, A.G. & Maciel, Y. 2024 Turbulent boundary layer response to uniform changes of the pressure force contribution. *arXiv preprint arXiv:2402.13067* .

Gungor, T.R., Maciel, Y. & Gungor, A.G. 2022 Energy transfer mechanisms in adverse pressure gradient turbulent boundary layers: production and inter-component redistribution. *Journal of Fluid Mechanics* **948**, A5.

Kitsios, V., Sekimoto, A., Atkinson, C., Sillero, J.A., Borrell, G., Gungor, A.G., Jiménez, J. & Soria, J. 2017 Direct numerical simulation of a self-similar adverse pressure gradient turbulent boundary layer at the verge of separation. *Journal of Fluid Mechanics* **829**, 392–419.

Maciel, Y, Wei, T., Gungor, A.G. & Simens, M.P. 2018 Outer scales and parameters of adverse-pressure-gradient turbulent boundary layers. *Journal of Fluid Mechanics* **844**, 5–35.

Sillero, J.A., Jiménez, J. & Moser, R.D. 2013 One-point statistics for turbulent wall-bounded flows at Reynolds numbers up to $\delta^+ \approx 2000$. *Physics of Fluids* **25** (10), 105102.